International Journal of Energy and Environmental Engineering
a SpringerOpen Journal

ORIGINAL RESEARCH Open Access

Experimental investigations of butanol-gasoline blends effects on the combustion process in a SI engine

Simona Silvia Merola*, Cinzia Tornatore, Luca Marchitto, Gerardo Valentino and Felice Esposito Corcione

Abstract

Fuel blend of alcohol and conventional hydrocarbon fuels for a spark-ignition engine can increase the fuel octane rating and the power for a given engine displacement and compression ratio. In this work, the influence of butanol addition to gasoline in a port fuel injection, spark-ignition engine was investigated. The experiments were realized in a single-cylinder ported fuel injection spark-ignition (SI) engine with an external boosting device. The optically accessible engine was equipped with the head of a commercial SI turbocharged engine with the same geometrical specifications (bore, stroke and compression ratio) as the research engine. The effect on the spark ignition combustion process of 20% and 40% of n-butanol blended in volume with pure gasoline was investigated through cycle-resolved visualization. The engine worked at low speed, medium boosting and wide-open throttle. Fuel injections both in closed-valve and open-valve conditions were considered. Comparisons between the parameters related to the flame luminosity and the pressure signals were performed. Butanol blends allowed working in more advanced spark timing without knocking occurrence. The duration of injection for butanol blends was increased to obtain a stoichiometric mixture. In open-valve injection condition, the fuel deposits on intake manifold and piston surfaces decreased, allowing a reduction in fuel consumption. BU40 granted the performance levels of gasoline and, in open-valve injection, allowed to minimize the abnormal combustion effects including the emission of ultrafine carbonaceous particles at the exhaust. In-cylinder investigations were correlated to engine out emissions.

Keywords: Optical diagnostics, Cycle-resolved visualization, PFI SI boosted engine, Butanol-gasoline blend, Injection timing

Background

Increasing global concern due to air pollution and to the limited oil reserves has generated much interest in the environmental friendly fuels alternative to petroleum-based fuels, in particular for the transport sector in which the energy consumption depends almost exclusively on fossil fuels. Several countries aim to use sustainable biofuels, which generate a clear and net GHG saving and have no negative impact on biodiversity and land use. In this scenario, butanol has strong potential as a biofuel. Like ethanol, butanol can be produced both by petrochemical and fermentative processes. The production of biobutanol by fermentation for use as a biofuel is generating considerable interest as it offers certain advantages in comparison with bioethanol. These include higher energy content, lower water adsorption and corrosive properties, better blending abilities and the ability to be used in conventional internal combustion engines without the need for modification. Biobutanol can be produced from starch or sugar-based substrates by fermentation (acetone-butanol-ethanol named ABE fermentation process).

However, cost issues, the relatively low yield and sluggish fermentations, as well as problems caused by end product inhibition and phage infections, meant that ABE butanol could not compete on a commercial scale with butanol produced synthetically, and almost all production ceased as the petrochemical industry evolved. However, the increasing interest in the use of biobutanol as a transport fuel induces a number of companies to explore novel alternatives to traditional ABE fermentation, which

* Correspondence: s.merola@im.cnr.it
Istituto Motori-CNR, Via Marconi 8, Naples, 80125, Italy

would enable biobutanol to be produced on an industrial scale.

Regarding the automotive use of biobutanol, the technology to make biobutanol, a nonfood-based biofuel, cost-competitive with fossil fuels isn't here yet, but several companies are working with this target. With respect to gasoline, butanol (or biobutanol) has a number of advantages over other common alcohol fuels such as ethanol and methanol. The energy density of gasoline is about 32 MJ/L, while butanol shows 29.2 MJ/L compared to ethanol, 19.6 MJ/L, and methanol, 16 MJ/L. This makes butanol so close to gasoline that it can allow a straight-across replacement in terms of energy [1]. Butanol is far less hygroscopic than methanol, ethanol and propanol. These lower alcohols are fully miscible with water, whereas butanol has only a modest water solubility. This allows a low-energy intermediate purification step [2]. Butanol is less corrosive than ethanol, can be transported in existing pipelines and is much safer to work with than lower alcohols based on its relatively high boiling point and flashpoint. In comparison with ethanol, the adding of butanol to conventional hydrocarbon fuels for use in a spark-ignition engine can increase fuel octane rating and power for a given engine displacement and compression ratio, thereby reducing fossil fuel consumption and CO_2 emissions [3-5]. Ethanol use has been widely investigated for spark-ignition engines, while few studies have been performed on butanol-gasoline combustion and on butanol-fueled engines [6,7]. Literature is particularly poor with respect to boosted spark-ignition (SI) engine experimental data. Almost all of the studies about butanol-gasoline blends consisted of the evaluation of performance, fuel consumption and exhaust emissions for different engine-operating conditions [6-10]. The in-cylinder process characterizations were principally realized through pressure measurements. These research activities demonstrated that the concentrations of 20% to 40% butanol in gasoline enabled to run the engine at a leaner mixture than gasoline for a fixed performance. These blends offered UHC emissions similar to gasoline, and they increased at higher butanol concentrations. The blends decreased the NO_x emissions to a lower level than with pure gasoline at its leanest mixture. The slight increase in specific fuel consumption (SFC) with the butanol addition was related to the blend's reduced combustion enthalpy. For example, B40 has a 10% lower combustion enthalpy than gasoline, which increases SFC of 10% for stoichiometric and slightly lean mixtures. It was measured that, by adding butanol, the coefficient of variation of indicated mean effective pressure (COV_{IMEP}) was reduced, particularly with lean mixtures, and the fully turbulent combustion phase (10% to 90% MFB) was similar in duration for all blends and pure gasoline. This latter finding showed that butanol has a similar or higher laminar flame speed than gasoline [6,11].

In recent works, the performance of a gasoline engine fuelled with gasoline-butanol blends of different mixing fractions was analyzed. It was demonstrated that butanol is a very promising alternative fuel with great potential for saving energy; a reduction of 14% in brake-specific energy consumption and emissions was observed [12].

Recent experimental investigations conducted using a single-cylinder spark-ignition research engine allowed comparing the performance and emissions of neat n-butanol fuel to that of gasoline and ethanol. It was found that gasoline and butanol are closest in engine performance, with butanol producing slightly less brake torque. Exhaust gas temperature and nitrogen oxide measurements show that butanol combusts at a lower peak temperature. Of particular interest were the emissions of unburned hydrocarbons, which were between two and three times to those of gasoline, suggesting that butanol is not atomizing as effectively as gasoline and ethanol [13].

At the same time, fundamental biobutanol combustion work was carried out; the oxidation of butanol-gasoline surrogate mixtures (85 to 15 vol.%) was studied using a jet-stirred reactor in the work by Dagaut and Togbé [14]. The aim of this paper is better comprehension of in-cylinder phenomena correlated with butanol-gasoline combustion in a SI engine. To this goal, cycle-resolved visualization was performed to follow the flame propagation from the spark ignition to the late combustion phase. The experiments were realized in a single-cylinder ported fuel injection (PFI) SI-boosted engine. The optically accessible engine was equipped with the cylinder head of a commercial SI turbocharged engine with the same geometrical specifications (bore, stroke and compression ratio) of the research engine. Butanol-gasoline blend was tested for several engine operating conditions. Changes in spark timing and fuel injection phasing were considered. Comparison between the parameters related to flame luminosity and to pressure signals were performed, and in-cylinder investigations were correlated to engine out emissions.

Methods

Experimental apparatus

The engine used for the experiments was an optically accessible single-cylinder PFI SI engine. It was equipped with the cylinder head of a commercial SI turbocharged engine with the same geometrical specifications. Further details on the engine are reported in Table 1. The head had four valves and a centrally located spark plug. The injection system was the same as the commercial one with a ten-hole injector. An external air compressor was used to simulate boosted conditions of intake air pressure and temperature

Table 1 Specifications of the single-cylinder ported fuel injection engine

Engine specifications	
Displaced volume	399 cc
Stroke	81.3 mm
Bore	79 mm
Connecting rod	143 mm
Compression ratio	10:1
Number of valves	4
Exhaust valve open	153 CAD ATDC
Exhaust valve close	360 CAD ATDC
Inlet valve open	357 CAD ATDC
Inlet valve close	144 CAD BTDC

ATDC, after top dead centre; BTDC, before top dead centre; CAD, crank angle degree.

in the ranges of 1,000 to 2,000 mbar and 290 to 340 K, respectively.

A quartz pressure transducer was flush-installed in the region between the intake-exhaust valves at the side of the spark plug. The transducer allowed performing in-cylinder pressure measurements in real time. An elongated engine piston was used; it was flat and its upper part was transparent since it was made of fused silica UV enhanced ($\Phi = 57$ mm). To avoid window contamination by the lubricating oil, self-lubricant Teflon-Bronze composite piston rings were used in the optical section.

To reduce the initial conditions effects, the engine was preheated by a conditioning unit, and it was maintained in motored condition by an electrical engine until the temperature reached 65°C. After the warm up, the engine worked in fired conditions for 300 consecutive cycles. The engine parameters and pressure measured in the last 200 cycles were considered in the work. Then the engine returned to motored condition for 100 cycles. This phase allowed checking a possible change in thermal and fluid dynamic status of the engine from the beginning of the measurements.

Figure 1 shows the experimental apparatus for the optical investigations and the bottom field of view of the combustion chamber. During the combustion process, the light passed through a quartz window located in the piston, and it was reflected toward the optical detection assembly by a 45°-inclined UV-visible mirror located at the bottom of the engine.

Cycle-resolved flame visualization was performed using an Optronis model CamRecord 5000 high-speed camera (Optronis GmbH, Kehl, Germany). It was a complementary metal oxide semiconductor (CMOS) monochrome image sensor; its full chip dimension was 512 × 512 pixel, and the pixel size was 16 × 16 μm. The camera A/D conversion was 8 bit, and the spectral range extended from 390 to 900 nm. The camera was equipped with a 50-mm focal Nikon lens (Nikon UK Ltd., Surrey, England); a camera region of interest was selected (480 × 480 pixel) to obtain the best match between spatial and temporal resolution. All the images are a line-of-sight average. The optical assessment allowed a spatial resolution in a 2D field of view around 120 μm/pixel. The exposure time was fixed at 10 μs, and the frame rate was 5,392 fps. In this work, the optical measurements were performed during 100 consecutive engine cycles after an engine warm up under motored conditions and 100 fired cycles. National Instruments LabVIEW acquisition system driven by an optical encoder with 0.2 crank angle degree resolution recorded the TTL signals from the high-speed camera acquisitions and the pressure transducer. In this way, it was possible to determine the crank angles at which the optical measurements were carried out. Finally, to quantify the variability of indicated work per cycle, the COV_{IMEP} was calculated.

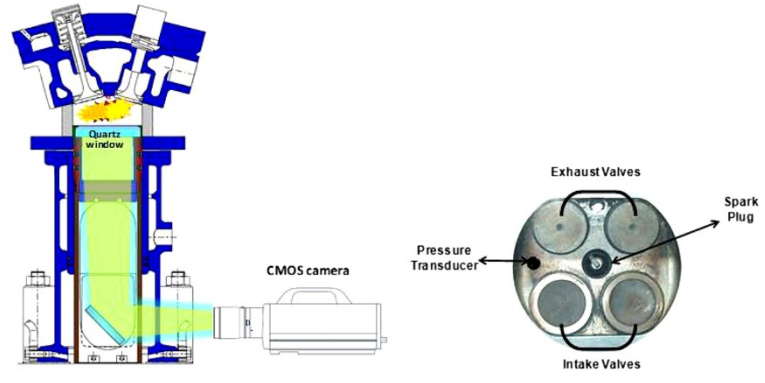

Figure 1 Experimental setup for optical measurements with bottom field of view of the combustion chamber.

In-house LabVIEW numerical procedures were applied for the retrieving of the optical data. The 8-bit gray-scale images were converted to numerical matrices. In this way, it was possible to evaluate the luminous signals locally or as integral on the whole combustion chamber. In a second procedure, a threshold was applied to each image. On the resulted binary images, a morphology function able to evaluate the mean radius of the flame front as distance between the combustion chamber center and the outline of the flame was applied.

Combustion tests were carried out using, as baseline fuel, the commercial gasoline; moreover, two blends with the volume of 20% and of 40% n-butanol with gasoline were tested. The blends were indicated in the following as BU20 and BU40, respectively. The main properties of the two fuels are reported in Table 2. Finally, steady-state measurements of HC, NO_x and soot were performed in the undiluted exhaust. Gaseous emissions were measured by an AVL Digas 4000 (AVL DiTEST, Graz, Austria) equipped with an electrochemical sensor for NO_x and nondispersive infrared analyzers for HC. Smoke was measured by a part flow opacimeter (AVL Opacimeter 439). The opacity can be directly correlated to the particulate mass concentration [15].

Results and discussion

All the tests presented in this paper were carried out at an engine speed of 2,000 rpm and wide-open throttle. Absolute intake air pressure and temperature were fixed at 1.4 bar and 338 K, respectively. The relative injection pressure was settled at 3.5 bar. The spark timing was changed in the range 12 to 20 crank angle degree before top dead centre (CAD BTDC) in order to identify the maximum brake torque and the knocking limit. To distinguish normal combustion cycles from knocking cycles, the knocking signal was evaluated through 5- to 30-kHz band-pass filtering of the pressure signals [16-18]. For all cycles, the evolution of the knock pressure was calculated using the absolute value of the knock signal. The combustion cycles were classified in the following way according to their knock intensity [19-21]:

- normal combustion (knock pressure 2% lower than the motored pressure at TDC),
- borderline knocking (knock pressure between 2% and 5% of the motored pressure),
- standard knocking (knock pressure between 5% and 25% of the motored pressure),
- heavy knocking (knock pressure was 25% higher than the motored pressure).

The duration of injection (DOI) was changed in order to set $\lambda = 1.0$ (±3%), as measured by a lambda sensor at the engine exhaust, and averaged over 200 consecutive engine cycles. The fuel injection conditions are resumed in Table 3. The injection timings were fixed at 130 CAD after top dead centre (ATDC) and 300 CAD BTDC in order to inject the fuel when the intake valves were closed (CV) and open (OV), respectively.

In a port-fuel-injected engine, the fuel is generally injected at the backside of a closed intake valve to take advantage of the warm valve and port surfaces for vaporization [22-24]. However, a large part of the injected spray is deposited on the intake manifold surfaces and forms a layer of liquid film on the valve and port surfaces. The film needs to be re-atomized by the shearing airflow as the intake valves open. If these fuel layers are not well atomized, they enter the cylinder as drops and ligaments [25-27]. These phenomena occur in varying degrees and depend upon the engine design, injector location and engine operation. Previous experiments on the same engine fuelled by gasoline and BU20 demonstrated that the injector sprayed the fuel towards the plate between the intake valves and on the intake valves stems [28-30]. The droplet impingement induced fuel layer formation on the intake manifold walls. The fuel layers were drawn by gravity to the valve head and gap, where they remained as film due to surface tension. The stripping of the squeezed fuel film created fuel

Table 2 Fuel specifications

	Gasoline	Butanol
Low heating value (MJ/kg)	43.5	32.1
Latent heat of vaporization (kJ/L)	223	474
Reid vapor pressure (kPa)	60 to 90	18.6
Stoichiometric air-to-fuel ratio	14.6	11.1
Density (kg/m^3)	720 to 775	813
Oxygen (wt.%)	<2.7	21.6
Research octane number	95	113
Adiabatic flame temperature (K)	2,370	2,340

Table 3 Fuel injection conditions

Label	Fuel	SOI	DOI
Gas_OV	gasoline	300 CAD BTDC	133 CAD
Gas_CV	gasoline	130 CAD ATDC	148 CAD
BU20_OV	BU20	300 CAD BTDC	145 CAD
BU20_CV	BU20	130 CAD ATDC	157 CAD
BU40_OV	BU40	300 CAD BTDC	153 CAD
BU40_CV	BU40	130 CAD ATDC	165 CAD

ATDC, after top dead centre; BTDC, before top dead centre; BU20, blend of 20% n-butanol with gasoline; BU40, blend of 40% n-butanol with gasoline; CAD, crank angle degree; CV, closed valve; DOI, duration of injection; Gas, gasoline; OV, open valve; SOI, start of injection.

deposits on the optical window. When the injection occurred in open-valve condition, part of the droplets was carried directly into the combustion chamber by the gas flow. These droplets, sucked in the combustion chamber, stuck on the cylinder walls. In both injection conditions, the fuel deposits on the combustion chamber walls created fuel-rich zones on the piston surfaces that influenced the composition of the mixture charge and, hence, the combustion process. During the normal combustion process, only a fraction of the fuel deposits was completely burned. Thus, more fuel should be injected to reach the selected air-fuel ratio measured at the exhaust [23].

In the open-valve injection, the fuel deposits amount and size were smaller than in the closed-valve injection; thus, the duration of injection resulted shorter [25,29]. Regarding the difference in the injection duration, as with any alcohol, gasoline-butanol blends have a lower stoichiometric air-fuel ratio. Therefore, when using gasoline blended with butanol, fuel flow must be increased to ensure the same relative air-fuel ratio as with pure gasoline.

In order to estimate the effect on engine performance of the selected fuel injection conditions, IMEP and COV_{IMEP} were evaluated as average on 100 consecutive engine cycles. For each spark timing, the IMEP variation was lower than 5% for all engine conditions and fuels. For each fuel, the IMEP of CV injection was higher than that of OV, in agreement with previous works [20,29]. For BU20, the IMEP in the OV condition was higher than gasoline in OV condition and very close to gasoline in CV condition. This occurred because butanol-gasoline blend burns faster than pure gasoline at the same conditions, making higher the indicated efficiency of the engine work cycle. For BU20_OV, the best stability was measured too [7]. This concurs with the results reported in the works by Irimescu [31] and Yang et al. [32] in which, at full load, the power drop is significant only for butanol concentrations higher than 30% to 40%. About the spark timing effect, for gasoline fuel, the knocking limit was evaluated around 16 CAD BTDC for both fuel injection conditions.

For BU20, the knocking limit was evaluated around 18 CAD BTDC, and for BU40, it advanced until around 20 CAD BTDC. It means that butanol blend allowed working in more advanced spark timing without occurrence of knocking combustion. The COV_{IMEP} increased with spark advance until reaching the highest value in knocking regime. From 16 CAD BTDC, the COV_{IMEP} increased with retarding spark timing too. This result agrees with those reported in the works by Szwaja and Naber [7] and Morey and Seers [33]. It occurs because, when the ignition is too advanced, the cylinder temperature is comparatively low. Besides, the quite low and uneven mixture concentration near the spark plug brings negative influence on the flame kernel initiation and development. When the ignition is too delayed, the low combustion efficiency does harm to combustion stability. In this work, the optical results obtained at 14 CAD BTDC spark timing are discussed. This choice was done in order to evaluate the effect of selected fuels on the normal combustion process at comparable IMEP (±1%) with satisfactory engine stability. Cycle-resolved visualization was used for detailing thermal and fluid dynamic phenomena that occur in the combustion chamber. Figures 2 and 3 report images of cycle-resolved flame front evolution for gasoline, BU20 and BU40 in CV and OV conditions. The images' brightness and contrast were changed to enhance the kernel flame luminosity. The combustion process was visualized from the spark ignition until the flame front reached the cylinder walls. As expected, for gasoline [29,31], after the evidence of the spark ignition, thanks to the plasma luminosity detected at 14 CAD BTDC, the flame front started as kernel from the spark plug, and then, it spread with radial-like behavior for around 6 to 10 CAD. Then, the flame front shape showed an asymmetry that induced the flame to reach first the cylinder wall in the exhaust valves region, around 20 CAD after the start of spark timing. This was due to the fuel film deposited on the intake valves and combustion chamber surfaces previously discussed. The fuel film develops dynamically under the effect of the gas flow, influencing mixture composition and combustion process. In fact, the flame propagation is influenced by the thermodynamic conditions, mixture composition and local turbulence intensity. When a flame propagates in the normal direction to a region with an equivalence ratio gradient, each part of the front evolves in a field with varying fuel concentration. This induces propagation speed variation along the flame front and an increase in flame wrinkling in comparison with the homogeneous case. A similar combustion process evolution was detected for both butanol blends.

As can be observed in Figure 2, the asymmetry was less evident for BU40, which showed a more regular evolution of the flame front with slight border wrinkling. This was a first marker of a lower amount of fuel deposits near the valves for the blend if compared to pure gasoline. Bright spots were observed in the burned gas before the flame front reached the chamber wall. The bright spots were due to the fuel deposits on the optical window. During the injection of fuel at closed intake valve, when the gas flow passes through the valves, the fuel droplets are stripped from the fuel film layer. After reaching the combustion chamber, the fuel droplets stuck on the piston surfaces. These fuel deposits also created fuel-rich zones that ignited when reached by the normal flame front. In CV condition, the spots are bigger

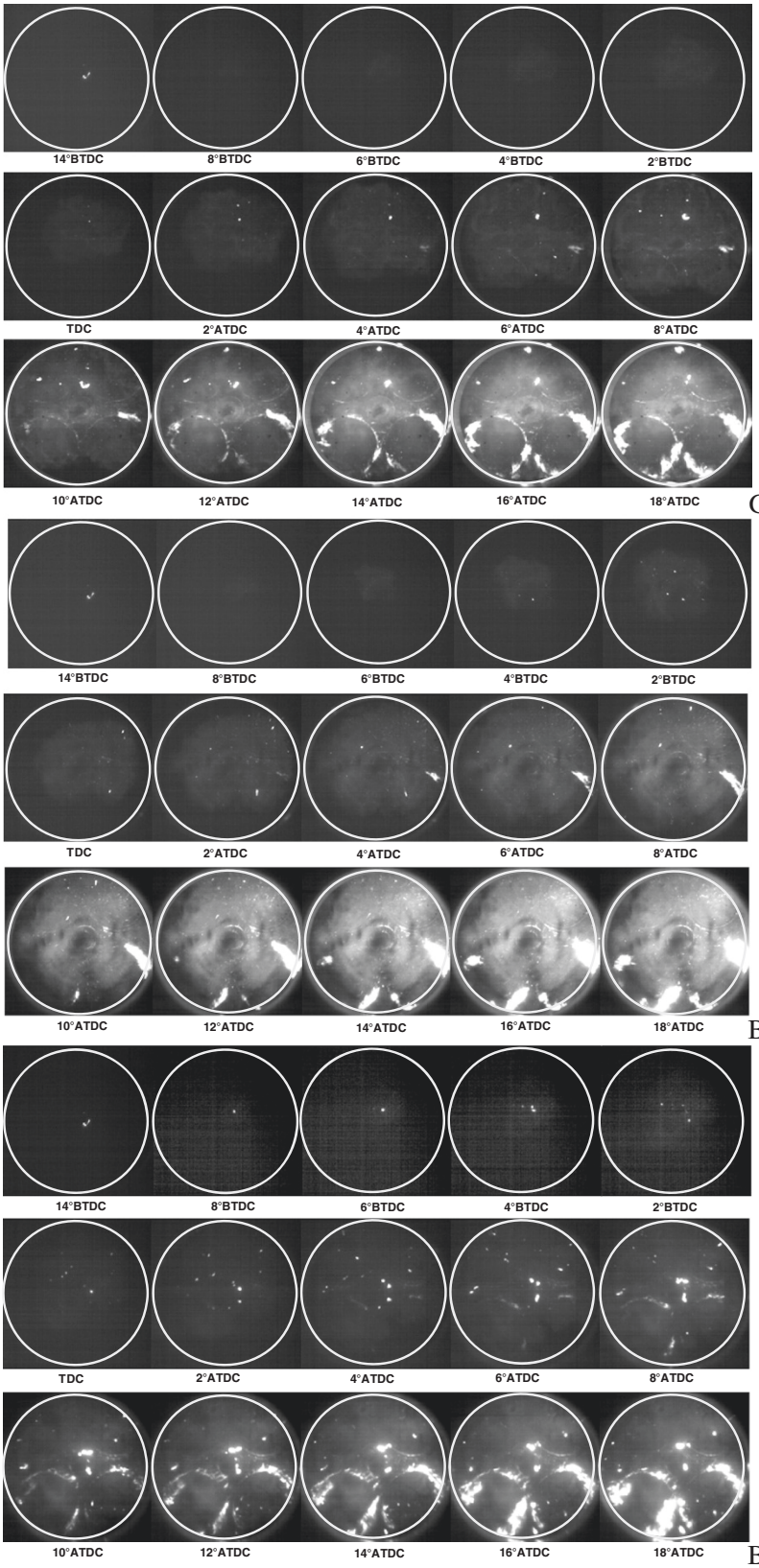

Figure 2 Cycle-resolved flame front evolution for gasoline, BU20 and BU40 in CV condition.

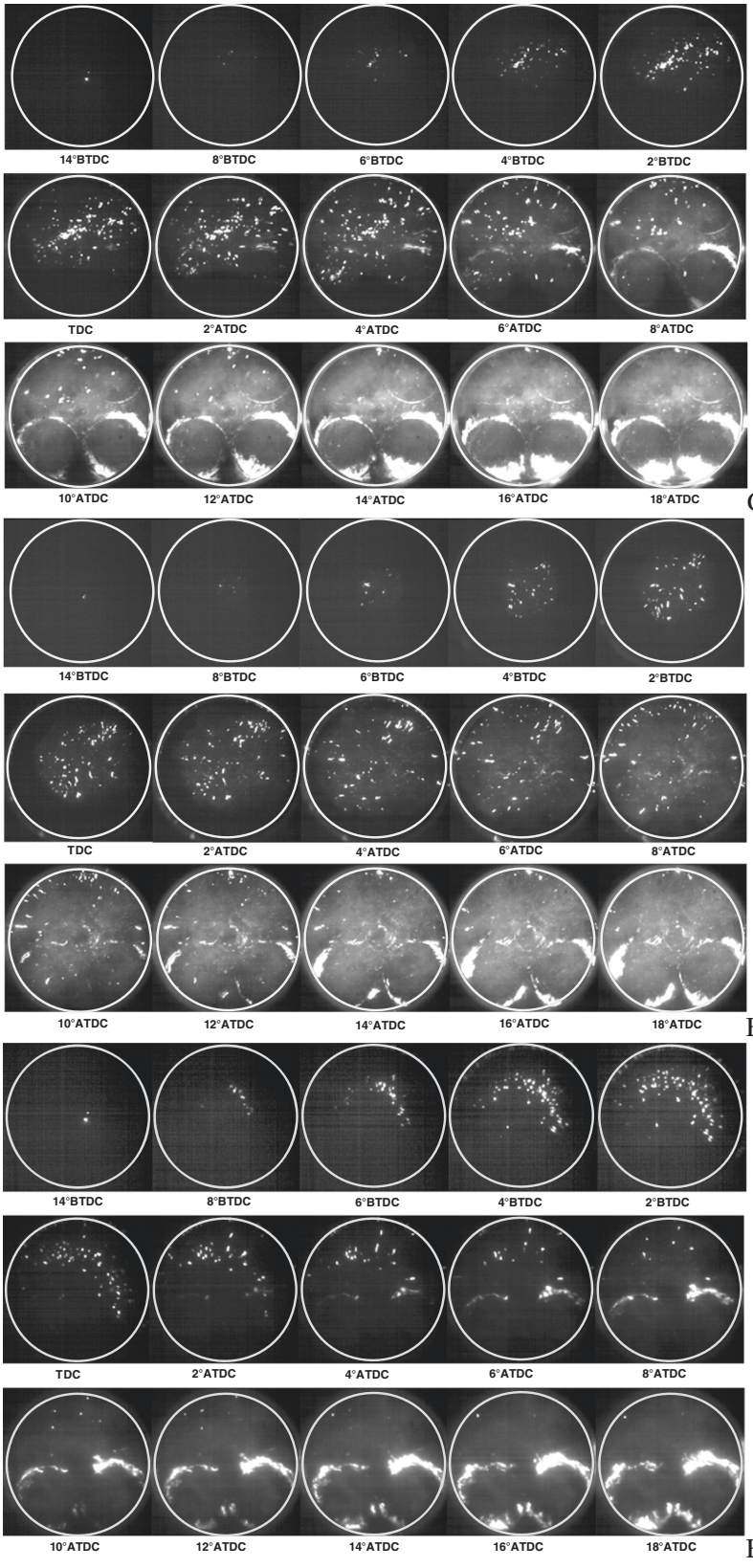

Figure 3 Cycle-resolved flame front evolution for gasoline, BU20 and BU40 in OV condition.

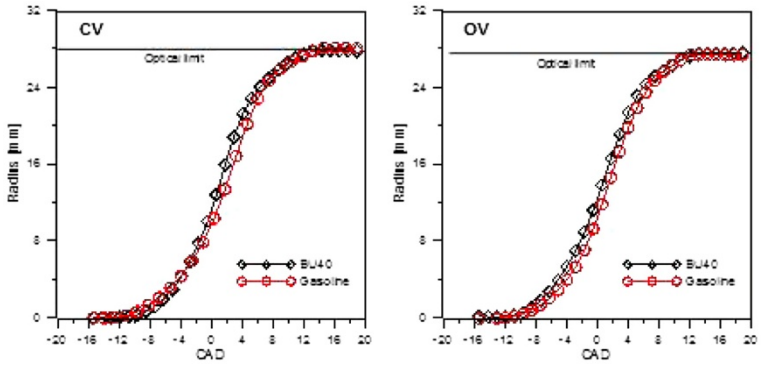

Figure 4 Evaluated flame radius of the 100 consecutive engine cycles.

but less in number than in OV condition. When the injection occurred in open-valve condition, the fuel droplets' sticking was enhanced by the partial carrying of the injected fuel droplets directly into the combustion chamber due to the gas flow. The bright spots have a random nature; during the combustion process, they decreased in size and number, and then, they disappeared before the exhaust valve opening [29]. The evidence of the bright spots decreased with the butanol percentage increasing. This means that the chemical composition of the blends helped the vaporization of the low-volatile component and then the fuel deposits burning. The presence of the fuel deposits, as squeezed film or impinged droplets, had direct effect on the flame radius evolution in terms of kernel cyclic variability and flame stability [25,34]. Figure 4 reports the trend of the flame radius for gasoline and BU40 evaluated on 100 consecutive cycles. Figure 5 shows the outline of the flame front evaluated for two CADs from the sequences of Figure 2. From its inception until around 6 CAD BTDC, the flame kernels had the same trends for both the fuels. Then, a little difference was observed; this was due to the reduced fuel amount deposited on the intake valves and on the piston surface that influenced the flame propagation. At around 4 to 6 CAD ATDC, flame radius evolution changed dramatically as shown in Figure 5 that shows the outline of the flame front evaluated from the sequences of Figure 2. This was due to approaching the intake valve region. In fact, the heat exchange between the intake ports and the surrounding gas led to the fuel film deposit evaporation. It influenced the composition of the mixture, creating locally fuel-rich zones. The higher fuel amount near the intake valves for gasoline in CV condition induced fuel-richer zones that slowed down the flame front more than in the other conditions.

When that normal flame front reached the intake valves, the fuel film layer around the valves burned, and strong-intensity flames were observed [35,36]. The

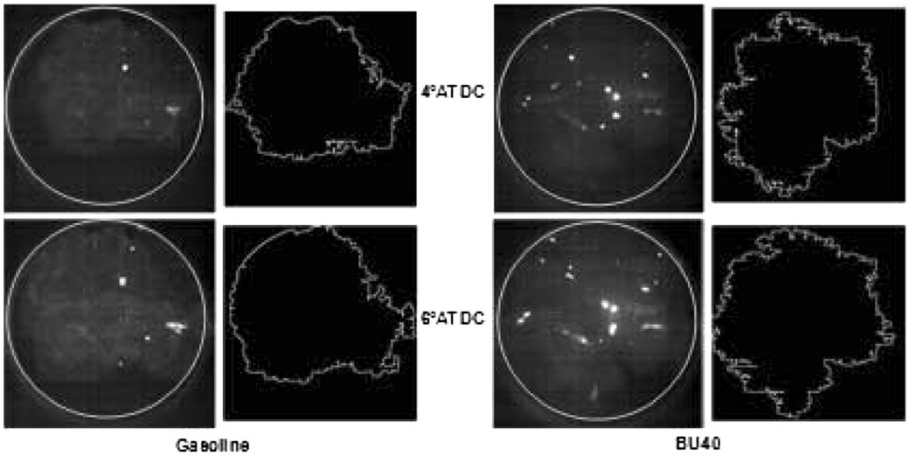

Figure 5 Flame fronts and related outlines evaluated from the sequences of Figure 2.

outlines of the valves are clearly distinguished since 8 CAD ATDC for all the tested conditions (Figures 2 and 3). Previous works demonstrated the presence of diffusion-controlled flames. Their inception was possible since the oxygen was not completely consumed after the normal flame front propagation [28,29,37]. The diffusion-controlled flames persisted in the late combustion phase, and their optical evidence could be detected until the exhaust valve opening.

The spatial distribution of diffusion-controlled flames can be analyzed through the images reported in Figure 6. For all fuels in closed valve injection condition, the resulting flames were more intense and have bigger surface than in open-valve condition due to the higher amount of fuel deposited on the valve stem for CV. Until 70 CAD ATDC, the highest intensity of the flames was observed near the intake valves, as expected, for all conditions. Then, different evolutions and spatial distributions were detected. This was in part due to the burning of fuel deposits carried by the gas motion from the intake to the exhaust valves. For BU40, the abnormal combustion was lower in intensity and duration. While for gasoline, the diffusion flame intensity decreased after 150 CAD ATDC due to the exhaust valve opening; for BU40, flame intensity were strongly reduced just around 130 CAD ATDC. Again, BU20 showed a mean behavior.

The abnormal combustion did not contribute to the engine work, and it did not influence the pressure signal [35]: it induced surface diffusion flames that warmed up the nearby in-cylinder gas by thermal diffusion. This phenomenon increased the pressure much slower than the reduction of pressure produced by the movement of the piston during the expansion stroke. A comparison between the pressure-related measurements and processed optical data was performed.

Figure 7 shows the evolution of the combustion pressure signal and the integral luminosity measured during the engine cycles of Figures 3 and 4. The combustion pressure signal was calculated by the subtraction of the motored in-cylinder pressure from the fired one. From the spark ignition to the maximum values, the luminous and pressure signals showed similar trends for all the fuels and injection conditions. The sharp increase was due to the chemical reactions occurring in the first moments of the combustion process that are exothermic and radiative in the wavelength range of the CMOS camera. Figure 8 reports typical spectra detected in the center of the combustion chamber in the early stage of the combustion process for gasoline fuel [37]. In Figure 8a, the results obtained at 7 CAD BTDC are shown. For both signals, the spectral features of OH and CH were detected [38-40]. In particular, the highest heads at 306 to 309 nm of the OH band system (250 to 320 nm) were well resolved. Excited OH radical was formed in the primary combustion zone by the chemiluminescent reaction: $CH + O2 \rightarrow CO + OH$. Moreover, the CH systems were observed near 431, 390 and 314 nm. The 431-nm band is the brightest; the 390-nm band system is very weak with closely packed heads. The 310-nm band is usually obscured by OH. In addition to the OH and CH features, a continuum on which two groups of diffuse bands were superimposed was detected. The first group was due to the Emeleus' bands of formaldehyde molecule CH_2O, and it had the highest emission in the range of 350 to 460 nm. The second band system identified the Vaidya's bands of HCO with the highest heads from 290 to 360 nm. Thus, the longer wavelength bands were overlapped by the CH_2O and continuum emission [39-41]. When the flame front overcame the spectroscopic measurement region, CH disappeared and high OH emission was measured, as shown in Figure 8b. Moreover, the burned gas is characterized by a broadband emission from UV to visible that is related to the CO_2 chemiluminescence [42]. Even if, in the flames, there is no sufficient energy to excite stable atoms or molecules to high electronic states, electronic states of CO_2 can be excited during the combustion by consecutive transitions from the ground state level to intermediate vibrationally activated levels [43,44]. The emission of CO-O appears as a continuum, which extends from 300 to 600 nm with a broad maximum around 375 nm.

The behavior of the combustion pressures and luminous intensities plotted in Figure 7 became quite different after the maximum around 20 CAD ATDC. For gasoline, the luminous signal decreased until a local minimum and then increased in the late combustion phase, while the pressure signal rapidly decreased. The diffusion-controlled flames greatly influenced the evolution of luminous signal, but their contribution to the combustion pressure was negligible. The diffusion flame intensity was higher for closed-valve injection than for open-valve due to the higher fuel amount deposition. For both conditions, the maximum was detected around 70 to 80 CAD ATDC. Previous investigations for gasoline fuel [37] showed that the diffusion-controlled flames were characterized by the optical markers of carbonaceous structures. Figure 8c reports typical spectra detected in the combustion chamber in the late combustion phase. The spectra presented a strong continuous contribution that increased with the wavelength in the visible range; this was representative of blackbody-like emission of soot precursors. Different levels of visible wavelength luminous intensity in the late combustion phase were related to different soot concentrations in the combustion chamber. The results confirmed those reported in the works of Witze and Green [36] and Kayes et al. [45] that assigned to the fuel deposition burning the cause of the volatile organic carbon compounds and ultrafine particles emission at the SI PFI exhaust. Regarding the

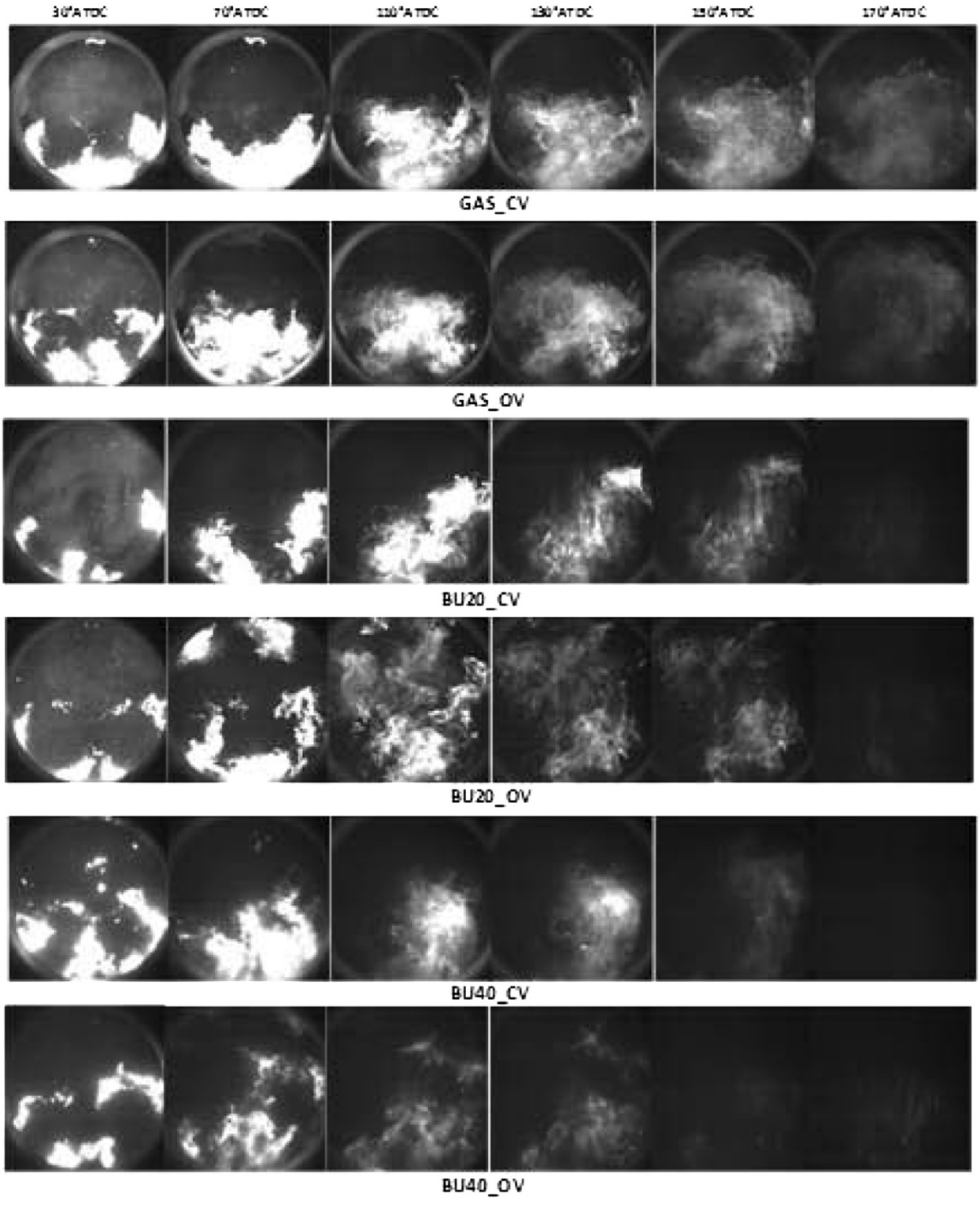

Figure 6 Cycle-resolved visualization of the late combustion phase.

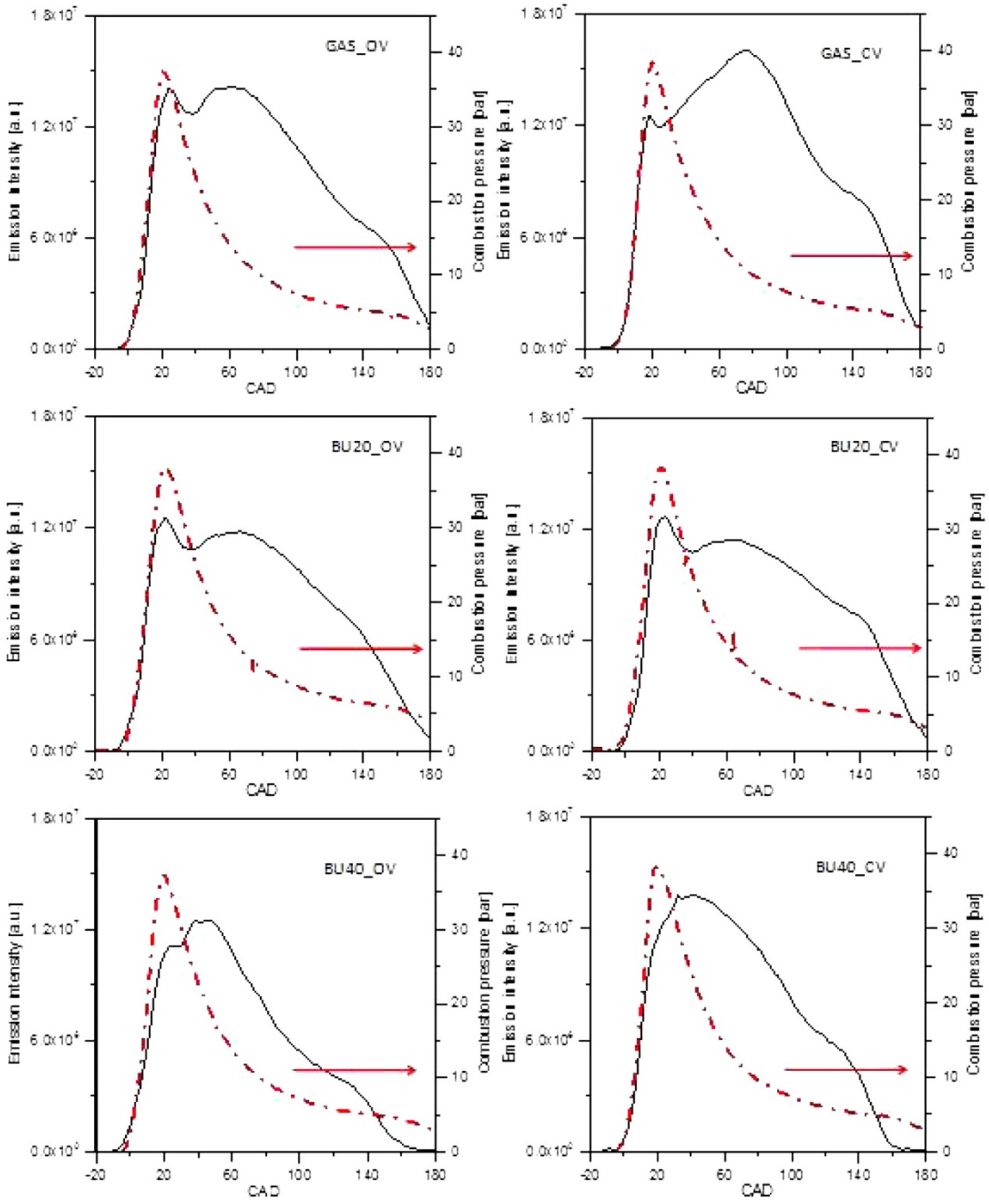

Figure 7 Evolution of the combustion pressure signal (dotted line) and the integral luminosity (solid line). Comparison between the net combustion pressure signal with the integral luminosity measured during the engine cycles of Figures 3 and 4.

temporal behavior of luminous signal, it should be noted that the spectra detected in the late combustion in Figure 8c showed a well-resolved signal due to OH radical that featured the soot oxidation phase [46]. OH emission was comparable for both fuel injection conditions. As a consequence, the open-valve condition showed not only a different spatial distribution of diffusion-controlled flame if compared to the closed-valve condition but also a more efficient soot oxidation phase. For butanol blends, the resulting integral luminosities in Figure 7 were less intense, demonstrating a lower particulate amount produced than gasoline with stronger soot reduction. This was more evident for BU40 due to higher oxygen content in the fuel. Even for butanol blends, higher particulate concentration

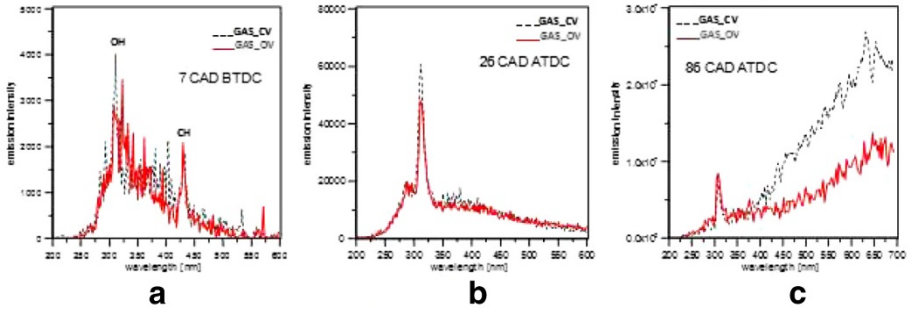

Figure 8 Typical spectra detected in the center of the combustion chamber for gasoline fuel [37]. (a) Results obtained at 7 CAD BTDC. **(b)** Measurement of high OH emission. **(c)** Typical spectra detected in the combustion chamber in the late combustion phase.

was detected for closed valve than for open one, as expected. At the exhaust valve opening, the soot reduction rate was not sufficient to complete the oxidation; thus, part of the particulate matter formed in the combustion chamber was emitted in the exhaust line. This result partially agrees with the opacity values measured at the undiluted exhaust and reported in Table 4. The discrepancy could be due to the sensitivity of the opacimeter to gaseous species such as heavy HC and NO_2 that have high absorption cross section [47,48] in the visible wavelength range that corresponds to the opacimeter working spectral region. It should be stressed that the absence of a catalyst device determined very high concentrations of HC and NO_x, and these can contribute to opacity value. Anyway, for all the tested fuels, HC in OV condition resulted higher than in CV. This occurred because, even if open-valve injection greatly reduces the amount of intake port wetting, it also induced larger in-cylinder wall wetting due to the direct fuel impingement. Experiments [49] showed that the many droplets associated with open-valve injection survived to the crank angle of ignition. This induced an inhomogeneous charge with poorer flame-front propagation that is responsible for reduction in performance and higher HC emission than closed-valve injection. Moreover, for small n-butanol blending (BU20), HC emissions were included among those of gasoline and BU40. The reduction with respect to gasoline was due to the decrease of the hydrocarbon fraction that led to the decrease of HC formation. The increase with BU40 could be due to the higher latent heat of vaporization than BU20. As reported in the work by Gu et al. [50], increasing butanol concentration in the blend with gasoline led to a decrease in the HC oxidation during expansion and exhaust processes.

Table 4 Engine out emissions

Label	HC (ppm)	NO_x (ppm)	Opacity (%)
Gas_CV	395	3,547	23.8
Gas_OV	458	3,749	15.1
BU20_CV	235	2,030	10.7
BU20_OV	408	2,905	9.3
BU40_CV	320	1,968	15.1
BU40_OV	433	2,528	11.5

BU20, blend of 20% n-butanol with gasoline; BU40, blend of 40% n-butanol with gasoline; CV, close valve; Gas, gasoline; OV, open valve.

Conclusions

The effect on the spark-ignition combustion process of n-butanol blended in volume with pure gasoline was investigated through cycle-resolved visualization applied in a single-cylinder PFI SI engine working at low speed, medium boosting and wide-open throttle. Two injection timings were fixed in order to inject the fuel at closed intake valve and open intake valve, respectively. The spark timing was changed to identify the maximum brake torque and the knocking limit. Blends of butanol up to 40% allowed working in more advanced spark timing without negative effects on performance. To work with a stoichiometric mixture for both fuels, the duration of injection was slightly increased for the blend. DOI in CV resulted longer than in OV for both fuels because, in CV injection, part of the injected spray is deposited on the intake manifold surfaces, forming a layer of liquid film. If these fuel layers are not well atomized, they enter the cylinder as drops and ligaments. During the normal combustion process, only part of the fuel deposits was completely burned. Thus, more fuel should be injected to reach the selected air-fuel ratio measured at the exhaust. When the normal flame front reached the fuel deposits, abnormal combustion was incepted. This was characterized by intense diffusion-controlled flames. Their contribution to the combustion pressure was negligible. The different levels of intensity were related to different carbonaceous structures and soot precursor concentrations. CV condition was characterized by higher fuel deposition amount and thus more intense diffusion-controlled flames than OV. Gasoline in CV condition showed the highest luminosity, and BU40 in OV condition, the lowest one. This demonstrated that

BU40_OV allowed the reduction of emission of ultrafine carbonaceous particles at the exhaust and the optimization of fuel consumption at fixed performance. Moreover, medium-low percentage of butanol in the gasoline allowed the reduction of NO_x and unburned hydrocarbon emission. Finally, even if an increase in the injected fuel amount should be considered to obtain the same air-fuel ratio for butanol-gasoline blend, if compared to pure gasoline, the better efficiency of fuel deposit burning allowed the reduction of that amount.

Acknowledgement
The authors would like to express their sincere appreciation to Mr. A. Mazzei for the precious technical support.

Competing interests
The authors declare that they have no competing interests.

Authors' contributions
SSM participated in the design of the study, performed the post processing of the data and drafted and corrected the manuscript. CT participated in the design of the study, carried out the experimental activity and helped in the organization and presentation of the data. LM participated in the design of the study, carried out the experimental activity and drafted the manuscript. GV participated in the design and coordination of the study and corrected the draft manuscript. FEC participated in the design and coordination of the study. All authors read and approved the final manuscript.

Authors' information
SSM received from the University of Naples in Italy her *Summa cum Laude* Magister Degree in Physics in 1995 and the PhD in Chemical Engineering in 2000. Since 2001, she is a full-position researcher in Istituto Motori of the Italian National Research Council. She specializes in the application of optical diagnostics to the combustion process investigation. Her research work focuses on the experimental analysis of the thermo fluid-dynamic phenomena that occur in-cylinder and at the exhaust of the internal combustion engines fuelled by conventional and alternative fuels. Since 1996, she has been involved with and has the direct responsibility for experimental activities in several national and international research projects.
CT received from the University of Naples in Italy her *Summa cum Laude* Magister Degree in Chemical Engineering in 2004 and PhD in Chemical Engineering in 2007. Her education activities were focused on the optical diagnostics of nanoparticles at internal combustion engine exhaust. From 2007 to 2011, she worked as associate researcher at Istituto Motori of the Italian National Research Council. Since 2011, she is a full-position researcher and is involved in research projects on the optical characterization of combustion process in internal combustion engines.
LM got his Mechanical Engineering MD at the University of Naples in Italy in 2006, working on fuel injection apparatuses for HD diesel engines. Since 2006, he is an associate researcher at Istituto Motori of the Italian National Research Council. His activity is mainly focused on fluid-dynamic characterization of sprays and high-injection pressure combustion by non-intrusive techniques using both mineral and biodegradable (first and second generation) fuels. He currently uses optical (Imaging, PDPA, PIV, UV–VIS chemiluminescence techniques) and non-conventional techniques (X-Rays) as well as forecast simulating codes to study mechanisms influencing the air/fuel mixture formation in internal combustion engines.
GV was born in 1957. He received his masters degree with honor in Mechanical Engineering from the University of Naples "Federico II" in 1980. He joined Istituto Motori (IM) of the National Research Council (CNR) as a researcher in 1984. In 2006, he was promoted to the rank of research manager and is currently overseeing one of the divisions of Istituto Motori focused on the mixture formation process and combustion within direct-injection engines. GV is an author of a large number of papers in qualified scientific conferences and magazines, with more than 20 years of expertise in optical diagnostics for fluid-dynamic and spray combustion research in internal combustion engines.
FEC received his degree in Electrical Engineering from the University of Naples "Federico II" in 1973. He joined Istituto Motori of the National Research Council in 1974 as a researcher. In 1991, he became research manager and, from 1997 to 2002, director of Istituto Motori. He is the chairman of the Executive Committee of International Energy Agency Implementing Agreement "Energy Conservation in Combustion and Emissions Reduction". He is the head of the Fluidynamics and Combustion Division of Istituto Motori, and he manages the research activity in thermodynamics, fluid mechanics, internal combustion engines and emission formation processes. He has published extensively in this field throughout the world (more than 270 papers). In 2000, he founded the SAE Naples Section. He is an SAE Fellow and a recipient of Distinguished Speaker of Japan Society of Automotive Engineers Award. From 2004 to 2008, he was a member of the SAE Board of Directors. In 1995 and 2008, he was a guest professor at the University of Wisconsin, Madison, USA. He was a guest professor at Wayne State University, Detriot, USA, in 2006 and at the University of Erlangen, Nurberg, Germany, in 2010.

Received: 23 November 2011 Accepted: 21 May 2012
Published: 21 May 2012

References

1. Veloo, PS, Wang, YL, Egolfopoulos, FN, Westbrook, CK: A comparative experimental and computational study of methanol, ethanol, and n-butanol flames. Combustion and Flame **157**(10), 1989–2004 (2010)
2. Ramey, DE: Continuous two stage, dual path anaerobic fermentation of butanol and other organic solvents using two different strains of bacteria. (1998). US Patent 5753474, 19 May 1998
3. Yacoub, Y, Bara, R, Gautam, M: The performance and emission characteristics of C1–C5 alcohol–gasoline blends with matched oxygen content in a single cylinder spark ignition engine. Proc. Inst. Mech. Eng. A. – Power. Energy **212**, 363–379 (1998)
4. Gautam, M, Martin, DW: Emission characteristics of higher-alcohol/gasoline blends. Proc. Inst. Mech. Eng. A. – Power. Energy **214**, 165–182 (2000)
5. Gautam, M, Martin, DW: Combustion characteristics of higher-alcohol/gasoline blends. Proc. Inst. Mech. Eng. **214A**, 497–511 (2000)
6. Dernotte, J, Mounaim-Rousselle, C, Halter, F, Seers, P: Evaluation of butanol–gasoline blends in a port fuel-injection, spark-ignition engine. Oil & Gas Science and Technology – Rev. IFP **65**(2), 345–351 (2010)
7. Szwaja, S., Naber, JD: Combustion of n-butanol in a spark-ignition IC engine. Fuel **89**, 1573–1582 (2010)
8. Alasfour, FN: Butanol - a single-cylinder engine study: availability analysis. Appl. Therm. Eng. Vol. **17**(6), 537–549 (1997)
9. Alasfour, FN: NOx emission from a spark-ignition engine using 30% iso-butanol – gasoline blend: Part 1: preheating inlet air. Appl. Therm. Eng. Vol. **18**(5), 245–256 (1998)
10. Alasfour, FN: NOx emission from a spark-ignition engine using 30 % iso-butanol – gasoline blend: Part 2: ignition timing. Appl. Therm. Eng. Vol. **18** (8), 609–618 (1998)
11. Broustail, G, Seers, P, Halter, F, Moréac, G, Mounaim-Rousselle, C: Experimental determination of laminar burning velocity for butanol and ethanol iso-octane blends. Fuel **90**, 1–6 (2011)
12. Yang, J, Wang, Y, Feng, R: The performance analysis of an engine fueled with butanol-gasoline blend. SAE Technical Paper (2011). doi:10.4271/2011-01-1191
13. Wigg, B, Coverdill, R, Lee, C-F, Kyritsis, D.: Emissions characteristics of neat butanol fuel using a port fuel-injected, spark-ignition engine. SAE Technical Paper (2011). doi:10.4271/2011-01-0902
14. Dagaut, P, Togbé, C: Oxidation kinetics of butanol–gasoline surrogate mixtures in a jet-stirred reactor: experimental and modeling study. Fuel **87**, 3313–3321 (2008)
15. Lapuerta, M, Martos, FJ, Cárdenas, MD: Determination of light extinction efficiency of diesel soot from smoke opacity measurements. Meas. Sci. Technol. Vol. **16**, 2048–2055 (2005)
16. Heywood, JB: Internal combustion engine fundamentals. McGraw-Hill, New York (1988)
17. Checkel, MD, Dale, JD: 1989. SAE Technical Paper (1989). doi:10.4271/890243
18. Brunt, MF, Pond, CR, Biundo, J: Gasoline engine knock analysis using cylinder pressure data. SAE Technical Paper (1998). doi:10.4271/980896

19. Mittal, V, Revier, BM, Heywood, JB: Phenomena that determine knock onset in spark-ignition engines. SAE Technical Paper (2007). doi:10.4271/2007-01-0007
20. Merola, SS, Sementa, P, Tornatore, C, Vaglieco, BM: Knocking diagnostics in the combustion chamber of boosted port fuel injection spark ignition optical engine. International Journal of Vehicle Design **49**(1–3), 70–90 (2009)
21. Merola, SS, Sementa, P, Tornatore, C: Experiments on knocking and abnormal combustion through optical diagnostics in a boosted spark ignition port fuel injection engine. International Journal of Automotive Technology **12**(1), 93–101 (2011)
22. Henein, NA, Tagomori, MK: Cold-start hydrocarbon emissions in port-injected gasoline engines. Progress in Energy and Combustion Science **25**, 563–593 (1999)
23. Behnia, M, Milton, BE: Fundamentals of fuel film formation and motion in SI engine induction systems. Energy Conversion and Management **42**(15–17), 1751–1768 (2001)
24. Costanzo, VS, Heywood, JB: Mixture preparation mechanisms in a port fuel injected engine. SAE Technical Paper (2005). doi:10.4271/2005-01-2080
25. Gold, MR, Arcoumanis, C, Whitelaw, JH, Gaade, J, Wallace, S: Mixture preparation strategies in an optical four-valve port-injected gasoline engine. Int. J. of Engine Research **1**(1), 41–56 (2000)
26. Nogi, T, Ohyama, Y, Yamauchi, T, Kuroiwa, H: Mixture formation of fuel injection systems in gasoline engines. SAE Technical Paper (1988). doi:10.4271/880558
27. Meyer, R, Heywood, JB: Liquid fuel transport mechanisms into the cylinder of a firing port-injected SI engine during start up. SAE Technical Paper (1997). doi:10.4271/970865
28. Merola, SS, Vaglieco, BM: Optical investigations of fuel deposition burning in ported fuel injection (PFI) spark-ignition (SI) engine. Energy **34**, 2108–2115 (2008)
29. Merola, SS, Sementa, P, Tornatore, C, Vaglieco, BM: Effect of injection phasing on valves and chamber fuel deposition burning in a PFI boosted spark-ignition engine. SAE International Journal of Fuels and Lubricants **1**(1), 192–200 (2009)
30. Merola, S, Tornatore, C, Valentino, G, Marchitto, L, Corcione, F: Optical investigation of the effect on the combustion process of butanol-gasoline blend in a PFI SI boosted engine. SAE Technical Paper (2011). doi:10.4271/2011-24-0057
31. Irimescu, A: Full load performance of a spark ignition engine fueled with gasoline -isobutanol blends. Analele Universităţii "Eftimie Murgu", Reşiţa **16** (1), 151–156 (2009)
32. Yang, J, Yang, X, Liu, J, Han, Z, Zhong, Z: Dyno test investigations of gasoline engine fueled with butanol-gasoline blends. SAE Paper (2009). doi:10.4271/2009-01-1891
33. Morey, F, Seers, P: Comparison of cycle-by-cycle variation of measured exhaust-gas temperature and in-cylinder pressure measurements. Applied Thermal Engineering **30**, 487–491 (2010)
34. Witze, P, Hall, M, Bennet, M: Cycle-resolved measurements of flame kernel growth and motion correlated with combustion duration. SAE Technical Paper (1990). doi:10.4271/900023
35. Zhu, GS, Reitz, RD, Xin, J, Takabayashi, T: Modelling characteristics of gasoline wall films in the intake port of port fuel injection engines. Int. J. Engine Research **2**(4), 231–248 (2001)
36. Witze, PO, Green, RM: LIF and flame-emission imaging of liquid fuel films and pool fires in an SI engine during a simulated cold start. SAE Technical Paper (1997). doi:10.4271/970866
37. Merola, SS, Sementa, P, Tornatore, C, Vaglieco, BM: Spectroscopic investigations and high resolution visualization of the combustion phenomena in a boosted PFI SI engine. SAE International Journal of Engines **2**(1), 1617–1629 (2009)
38. Gaydon, AG: The Spectroscopy of Flames. Chapman and Hall Ltd, London (1957)
39. Alkemade, CTJ, Herrmann, R: Fundamentals of Analytical Flame Spectroscopy. Hilger, Bristol (1979)
40. Dieke, GH, Crosswhite, HM: The ultraviolet bands of OH. J. Quant. Spectrosc. Radiat. Transfer **2**, 97–199 (1962)
41. Gaydon, AG, Wolfhard, HG: Mechanism of formation of CH, C2, OH and HCO radicals in flames. Symposium (International) on Combustion **4**(1), 211–218 (1953)
42. Samaniego, JM, Egolfopoulos, FN, Bowman, CT: CO2* chemiluminescence in premixed flames. Combust. Sci. and Tech. **109**, 183–203 (1995)
43. Gaydon, AG: The flame spectrum of carbon monoxide. In: (ed.) Proceedings of the Royal Society of London. Series A, Mathematical and Physical Sciences, vol. 176(967), pp. 505–521. Royal Society Publishing, London (1940)
44. Dixon, RN: In: (ed.) Proceedings of the Royal Society of London. Series A, Mathematical and Physical Sciences, vol. 275(1362), pp. 431–446. Royal Society Publishing, London (1963)
45. Kayes, D, Hochgreb, S: Mechanisms of particulate matter formation in spark-ignition engines 1. Effect of engine operating conditions. Environ. Sci. Technol. **33**, 3957–67 (1999)
46. Nagle, J, Strickland-Constable, RF: Oxidation of carbon between 1000°-2000°C. In: (ed.) Proceedings of the 5th Conference on Carbon, vol. 1, pp. 154–164. Pergamon Press, Oxford (1962)
47. Orphala, J, Chanceb, K: Ultraviolet and visible absorption cross-sections for HITRAN. Journal of Quantitative Spectroscopy & Radiative Transfer **82**, 491–504 (2003)
48. Verstraete, L, Leger, A: The visible and ultraviolet absorption of large polycyclic aromatic hydrocarbons. Astronomy and Astrophysics **266**(1), 513–519 (1992)
49. Chappuis, S, Cousyn, B, Posylkin, M, Vannobel, F, Whitelaw, JH: Effects of injection timing on performance and droplet characteristics of a sixteen-valve four cylinder engine. Experiments in Fluids **22**(4), 336–344 (1997)
50. Gu, X, Huang, Z, Cai, J, Gong, J, Wu, X, Lee, C: Emission characteristics of a spark-ignition engine fuelled with gasoline-n-butanol blends in combination with EGR. Fuel **93**, 611–617 (2012)

doi:10.1186/2251-6832-3-6
Cite this article as: Merola *et al.*: Experimental investigations of butanol-gasoline blends effects on the combustion process in a SI engine. *International Journal of Energy and Environmental Engineering* 2012 **3**:6.